Solar Physics (2025) 300:25
https://doi.org/10.1007/s11207-025-02449-5

RESEARCH

Two-Part Interplanetary Type II Solar Radio Bursts

Silja Pohjolainen[1]

Received: 20 December 2024 / Accepted: 25 February 2025 / Published online: 4 March 2025

Abstract
Two similar-looking, two-part interplanetary type II burst events from 2003 and 2012 are reported and analysed. The 2012 event was observed from three different viewing angles, enabling comparisons between the spacecraft data. In these two events, a diffuse wide-band type II radio burst was followed by a type II burst, which showed emission at the fundamental and harmonic (F-H) plasma frequencies, and these emission bands were also slightly curved in their frequency-time evolution. Both events were associated with high-speed, halo-type coronal mass ejections (CMEs). In both events, the diffuse type II burst was most probably created by a bow shock at the leading front of the CME. However, for the later appearing F-H type II burst, there are at least two possible explanations. In the 2003 event, there is evidence of CME interaction with a streamer, with a possible shift from a bow shock to a CME flank shock. In the 2012 event, a separate white-light shock front was observed at lower heights, and it could have acted as the driver of the F-H type II burst. There is also some speculation on the existence of two separate CMEs, launched from the same active region, close in time. The reason for the diffuse type II burst being visible only from one viewing direction (STEREO-A) and the ending of the diffuse emission before the F-H type II burst appears still need explanations.

Keywords Radio bursts · Coronal mass ejections · Initiation and propagation

1. Introduction

Solar radio bursts of type II appear as frequency-drifting emission lanes in radio dynamic spectra, with a drift from high to low frequencies. They can be observed at decimeter–meter wavelengths (Kumari et al. 2023) with ground-based telescopes, and from decameter to kilometer waves (Gopalswamy, Mäkelä, and Yashiro 2019) with space instrumentation. Space observations at frequencies lower than 15 MHz are often called interplanetary.

The frequency drift is generally thought to imply a propagating shock wave in the solar atmosphere, where the decreasing plasma frequency $f_p = 9000\sqrt{n_e}$ (in Hz) is caused by the decreasing electron density n_e (in cm^{-3}) along the transient or shock driver path (Dulk 1985). Plasma emission is generated by escaping radiation near the local plasma frequency

✉ S. Pohjolainen
silpoh@utu.fi

[1] Tuorla Observatory, Department of Physics and Astronomy, University of Turku, Turku, Finland

or its harmonics in a multistage process that includes Langmuir turbulence and its nonlinear evolution (Melrose 1987; Mann et al. 2022). Type II bursts can often be identified from the fundamental-harmonic (F-H) emission lane pairs, but harmonic emission is not always observed. At meter wavelengths, harmonic emission is typically stronger in intensity than fundamental, but at longer wavelengths the opposite can be observed. At kilometer waves, type II bursts are characterized by the absence of clear harmonic structure (Cane and Erickson 2005; Chernov and Fomichev 2021).

A distinct class of type II bursts that shows single-lane, diffuse emission with a wide frequency band was reported by Bastian (2007). Cane and Erickson (2005) had already noted that single-lane, broad-band interplanetary (IP) type II bursts are common in connection with fast and large CMEs. Bastian (2007) suggested that the emission may not be due to plasma radiation at all, but instead, it could be due to incoherent synchrotron radiation from near-relativistic electrons that are trapped within a fast-moving coronal mass ejection (CME) or sheath. The directionality of emission could be significant for plasma radiation, but it is not expected for synchrotron emission if the electron distribution function is nearly isotropic. Synchrotron emission would also fade away and cease in a certain time frame, as the magnetic field strength is decreasing in the IP space. In case of long-duration events, if the synchrotron-emitting electrons are shock-accelerated, then the electron energies would need to increase constantly to compensate for the magnetic field.

After the first speculation on the emission mechanism, wide-band type II bursts were studied further, for example with a statistical sample from 2001 – 2011 (Pohjolainen, Allawi, and Valtonen 2013). Almost all of the analysed 25 wide-band type II bursts were associated with very high-speed CMEs which originated from different parts of the solar hemisphere, i.e., no directional effects were found. From the data set, 18 bursts were estimated to have radio source heights that corresponded to the CME leading front heights, suggesting that they were created by bow shocks ahead of the CMEs. It was further suggested that the wide-band and diffuse type II bursts were formed when specific CME leading edge structures and/or special shock conditions were present.

In the Bastian (2007) event, the diffuse single-lane emission (named type II-S) was followed by an F-H emission lane pair (named type II-P), dividing the event into two parts. At least the later part of the burst thus indicated plasma radiation. The emission of the lane pair was also slightly curved in frequency, i.e., the frequency drift made a turn to higher frequencies, instead of drifting steadily toward lower frequencies.

Curved and fragmented structures within decimetric–metric type II bursts have been reported by, e.g., Pohjolainen, Pomoell, and Vainio (2008). In this particular case, numerical magnetohydrodynamic (MHD) simulations showed that this kind of type II burst emission can be created when a coronal shock, driven by a CME, passes through a system of dense loops. As the radio emission reflects the varying loop densities and the densities in between the loops (atmospheric background), the result is drifts and shifts within the F-H emission lanes. The speed of the shock driver determines the overall frequency drift of the burst, but the effects of the changing densities are superposed on this emission. In IP type II bursts, shifts and jumps to higher frequencies have also been observed (Al-Hamadani, Pohjolainen, and Valtonen 2017). One plausible explanation is CME shock interaction with a streamer (Feng et al. 2012), but basically any coronal density variation along the propagation path will affect the shape of the radio emission in the dynamic spectrum.

In addition to radio type II bursts, also radio type IV bursts are associated with CMEs. At decimeter–meter wavelengths they imply the lift-off stage of a CME, with emitting electrons trapped within magnetic structures. At longer wavelengths, the outward-moving plasmoid can create continuum emission that consists of both synchrotron emission from the trapped

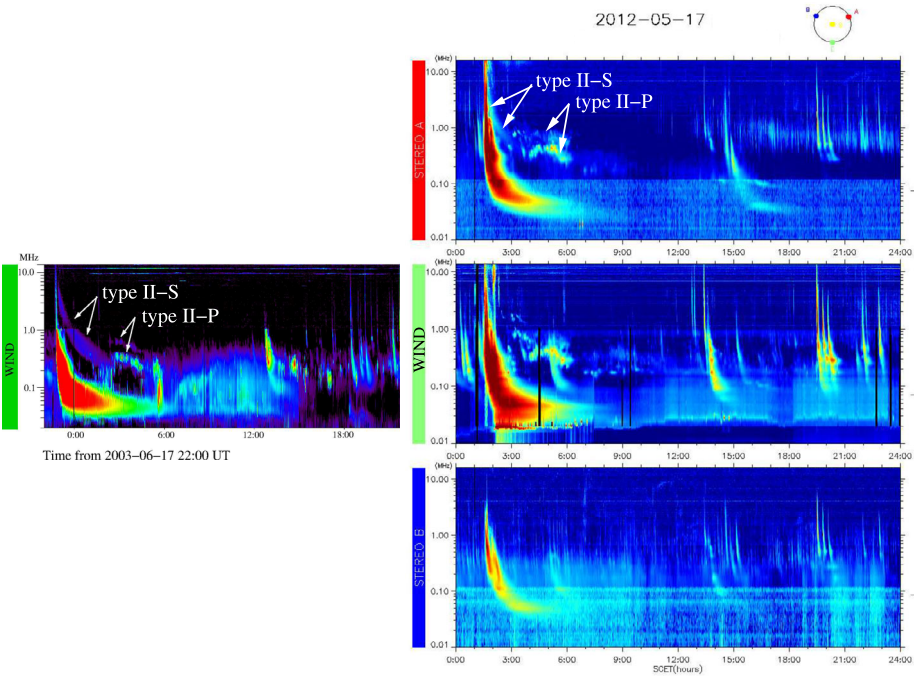

Figure 1 Observations of radio type II burst events on 17 – 18 June 2003 (*left*) and on 17 May 2012 (*right*). Both show a diffuse wide-band type II burst, marked type II-S, followed by a fundamental-harmonic emission lane pair, marked type II-P, as in Bastian (2007). The 2012 event could be observed from three different viewing angles from three spacecraft. The spacecraft positions are shown in the drawing (*top right corner* in the plot). A 24-hour period in the dynamic spectra is shown for both events.

electrons and plasma emission created by the propagating transient (Hillaris, Bouratzis, and Nindos 2016; Mohan et al. 2024). Large-scale EUV waves (Mann, Warmuth, and Önel 2023) and dimmings (Jin et al. 2022) have been associated with CMEs and radio type II and type IV bursts.

The two-part burst on 17 – 18 June 2003 analysed by Bastian (2007) could have been a single one event if no other similar events are observed. However, an almost identical-looking event occurred on 17 May 2012. The similarity of these events is most obvious when looking at the STEREO-A/SWAVES dynamic spectrum on the 2012 event and comparing it with the *Wind*/WAVES spectrum on the 2003 event; see Figure 1. For the 2012 event, it is possible to analyse radio observations from three different viewing angles using STEREO-A, STEREO-B, and *Wind* radio data, and compare their data with white-light and extreme ultraviolet (EUV) imaging observations. This study aims to find out why these events look so similar and what could be the reason for the two-part radio emission structures.

Observing instruments and data are described in Section 2. Observations of flares, CMEs, energetic particles, and shock arrivals are summarised in Section 3. Section 4 describes the radio emission features, explains how radio source heights are determined, and compares them with imaging observations at other wavelengths. In Section 5, we summarise our findings and discuss their relevance. In Section 6, we consider other issues related to this research topic.

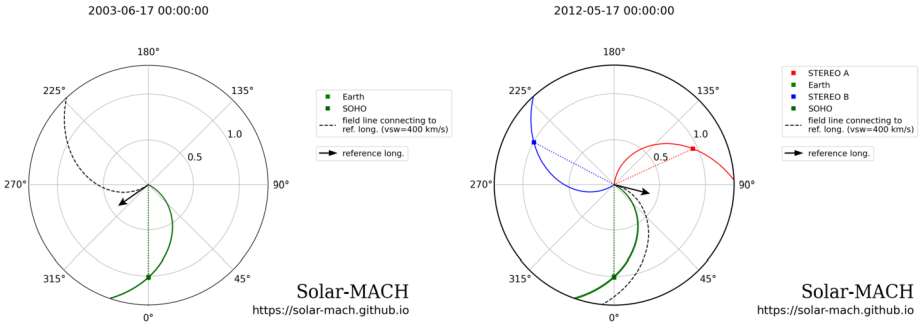

Figure 2 Solar-MACH plots for 17 June 2003 (*left*) and 17 May 2012 (*right*). *Black arrows* indicate the flare longitudes, and *black dashed lines* their magnetic connectivities.

2. Observations and Data

For the 2003 radio event, only one viewing direction was available from the L1 location along the Sun–Earth line. For the 2012 event, radio dynamic spectra were taken from three different locations from three spacecraft orbiting the Sun, and we could compare the radio spectral characteristics with EUV and white-light images obtained from these same locations.

From the location of L1, *Solar and Heliospheric Observatory* (SOHO) spacecraft (Domingo, Fleck, and Poland 1995) provides extreme ultraviolet (EUV) imaging of the solar disc with the *Extreme ultraviolet Imaging Telescope* (EIT). SOHO also provides coronagraph images taken with the *Large Angle and Spectrometric Coronagraph* (LASCO) C2 and C3 instruments, up to 32 $R_{\odot}$ distances. The *Solar Terrestrial Relations Observatory Ahead and Behind* (STEREO A and B) twin spacecraft (Kaiser et al. 2008) carry five *Sun Earth Connection Coronal and Heliospheric Investigations* (SECCHI) imagers. The SECCHI imagers include *Extreme Ultraviolet Imager* (EUVI), which provides EUV images of the solar disc, two coronagraphs COR1 and COR2, which provide Sun-centered images up to a distance of 15 $R_{\odot}$, and two heliocentric imagers HI1 and HI2, which provide white light images from the outer part of COR2 field of view, up to a distance of Earth orbit.

Images and associated data products were obtained from the CDAW LASCO CME Catalog at cdaw.gsfc.nasa.gov and by using the data and software in JHelioviewer (Müller et al. 2017).

Radio dynamic spectra at decimeter–meter wavelengths can be obtained from ground-based observatories. At decameter–hectometer (DH) wavelengths dynamic spectra can be obtained from *Wind*/WAVES (Bougeret et al. 1995) located in L1, close to SOHO with the same field of view. STEREO/SWAVES instrumentation (Bougeret et al. 2008) in the two STEREO spacecraft are very similar to the *Wind*/WAVES instruments.

For the 2003 event, only *Wind*/WAVES observations are available from Earth view. In 2012, also STEREO-A and STEREO-B made radio observations from two different positions. The separation angles between Earth and the spacecraft were 114.8° (Earth–A) and 117.6° (Earth–B), and the angle between A and B was 127.5°. The spacecraft positions at the event times are indicated in Figure 2, which also shows flare locations in the two events, with the available observing directions.

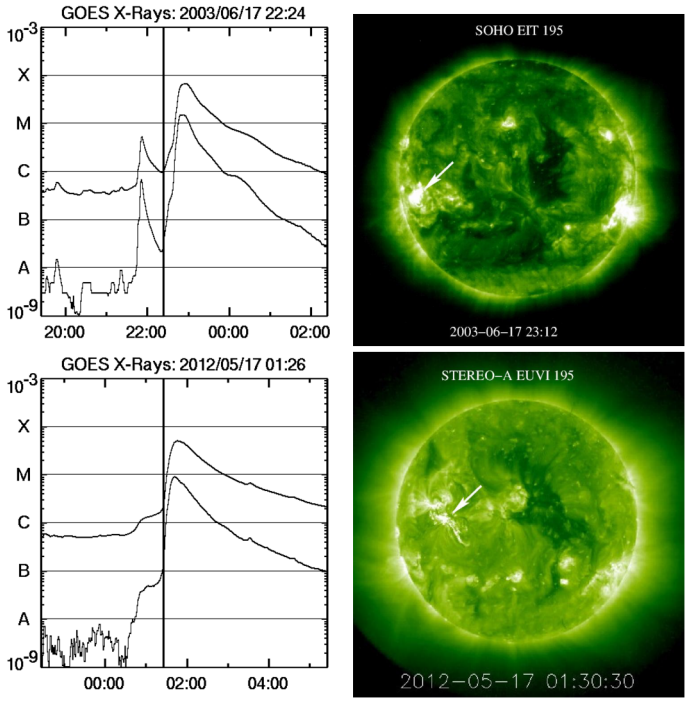

Figure 3 Flare intensities in soft X-rays observed by GOES (Earth view). The 2003 flare was located at S07E55, and the 2012 flare at N11W76. In STEREO-A view the 2012 flare occurred near N11E42. The flare locations are indicated with *arrows* in the EUV images, observed by SOHO/EIT and STEREO-A/EUVI at 195 Å wavelength.

3. Event Descriptions

3.1. Flares

The origin of the 17 – 18 June 2003 event was a flare located at S07 E55 in AR 10386. The flare was listed to start at 22:27 UT and peak at 22:55 UT. The flare intensity was GOES class M6.8. The flare was preceded by a GOES C5.2 flare in the same region, which was listed to start at 21:44 UT and peak at 21:53 UT. The GOES plot in Figure 3 shows that in X-rays the M6.8 flare starts in the intensity fall phase of the C5.2 flare. The SOHO/EIT 195 Å image shows the flare location at S07E55 (Earth view). No clear EUV wave was observed.

The 17 May 2012 event was associated with a flare located at N11 W76 in AR 11476. In STEREO-A view the flare was located approximately at N11 E42. The flare was listed to start at 01:25 UT and peak at 01:47 UT. The flare had GOES class M5.1 intensity (Earth view). The STEREO-A/EUVI 195 Å image in Figure 3 shows the flare location near N11E42. The flare was associated with an EUV wave that was best observed from STEREO-A.

3.2. CMEs

Both events were associated with fast halo-type CMEs. On 17 – 18 June 2003 the halo CME speed, from a linear fit to the leading front listed in the LASCO CME Catalog, was 1812 km s^{-1}, and the speed remained approximately the same during the observations.

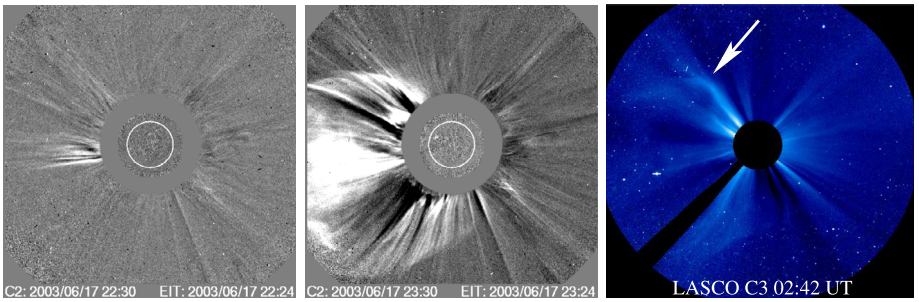

Figure 4 SOHO/LASCO-C2 difference images at 22:30 and 23:30 UT on 17 June 2003. The narrow-width eastward CME structure at 22:30 UT originated from the C5.2 flare. At 23:30 UT the front of the halo CME, associated with the M6.8 flare, had already passed the LASCO-C2 field of view. At 02:42 UT the LASCO-C3 image shows a bending of a streamer (location indicated with an *arrow*).

The CME leading front was first observed by SOHO/LASCO-C3 on 17 June 2003 at 23:18 UT, at height 7.06 $R_\odot$. This late first-observed height was due to a gap in C2 observations. Figure 4 shows two LASCO-C2 difference images, at 22:30 UT and 23:30 UT. At 22:30 UT a narrow-width bright structure preceded the halo CME, but it was not listed as a separate CME. At 23:30 UT the halo CME front had already passed the C2-instrument field of view.

Several streamers are visible in the coronagraph images. The streamer on the north-eastern side of the CME looks to be affected from 02:42 UT onward on 18 June 2003.

On 17 May 2012 the linear fit CME speed was 1582 km s^{-1}. The halo CME was decelerating, with a last-observed speed of 1320 km s^{-1} at height 26 $R_\odot$.

The CME front was first observed by SOHO/LASCO on 17 May 2012 at 01:48 UT, at height 3.61 $R_\odot$, but STEREO-A/COR1 observed the CME front already at 01:40 UT, at height 2.05 $R_\odot$. The observed CME heights from STEREO-A were, and also remained, lower than the LASCO CME heights. The CME heights observed from STEREO-B were even lower. From the height differences and spacecraft positions we can conclude that the CME was propagating to a direction in between Earth/SOHO and STEREO-A (both observed the leading front projected on the sky). STEREO-B did not observe the actual front as it was moving away on the opposite side of the Sun. Streamers were also present on both sides of the expanding CME.

The eruptions in this 2012 solar event have been studied by Shen et al. (2013) and more recently by Grechnev et al. (2024). Shen et al. (2013) suggested that there were two eruptions that originated from the same active region close in time, within minutes, and they formed two separate CMEs. They used the Graduated Cylindrical Shell (GCS) model to study how the two CMEs propagated. CME1 was outlined as a halo (indicated with a red line in Figure 5), and CME2 was propagating sideways in a more narrow cone (green line in Figure 5). According to Shen et al. (2013), in the STEREO-A observations, these structures overlap and appear to be propagating together. Shen et al. (2013) also proposed that there were two separate shocks caused by the two CMEs.

Grechnev et al. (2024) studied these eruptions further, and they also identified two separate eruptions, but now located behind a CME-bubble front. In their interpretation, this led to two propagating wave-like disturbances within one expanding CME. The two disturbances later merged into a single, stronger, and faster shock, a wave-halo (location indicated with a dashed yellow line in Figure 5). At heights exceeding ten solar radii, after 03:00 UT,

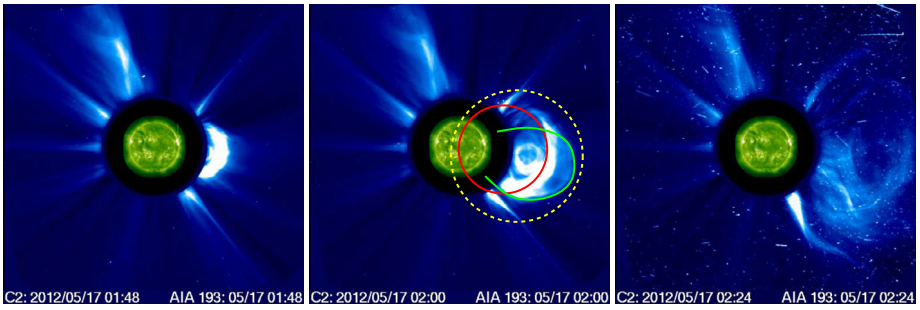

Figure 5 CME event on 17 May 2012, from SOHO/LASCO-C2 observations at 01:48 UT, 02:00 UT, and 02:24 UT. In the 02:00 UT image the two CMEs suggested by Shen et al. (2013) are outlined roughly with *red* (CME1) and *green* (CME2) *lines*. The *yellow dashed line* approximates the location of the wave-halo suggested by Grechnev et al. (2024). The most-affected streamer is located on the south-western side of the CME.

the wave-halo front looked to fall behind the fastest LASCO CME-body front. So, in some aspects, this solar event still remains unclear.

3.3. Energetic Particles and Interplanetary Transients

Intense flares and shock waves associated with fast CMEs have been named as the source of solar energetic particle (SEP) events, where protons are accelerated to relativistic energies. They can also cause a signal in ground-based detectors like neutron monitors. These are called ground level enhancement (GLE) events. Propagating shock waves and interplanetary CMEs (ICME) can be observed in-situ, as they change the local plasma parameters. The database of interplanetary shocks is at ipshocks.helsinki.fi/. ICME observations from 2007 – 2016 using the STEREO spacecraft are available at stereo-ssc.nascom.nasa.gov/pub/ins_data/impact/level3/; see also Jian et al. (2018). In ICME-related shocks, the shock arrival is followed by the magnetic cloud passage.

The 17 – 18 June 2003 burst source was not well connected to Earth, as it was located near the solar east limb. The event was not listed as a GLE event, but it was a proton event with proton flux of 24 pfu at energies > 10 MeV; see the NOAA SEP event list at umbra.nascom.nasa.gov/SEP/.

Wind observed shock arrival on 20 June 2003 at 08:02 UT, with shock speed 638 km s^{-1}. The travel time from the Sun to the spacecraft would be 57 hours, with mean speed of 725 km s^{-1}.

The 17 May 2012 burst source was located near the west limb, with very good connection to Earth; see the magnetic field lines in the Solar-MACH plots in Figure 2. The event was a GLE event number 71, the first of only two GLEs to occur in Solar Cycle 24. Several studies have investigated the SEP acceleration in this event using the available multispacecraft in situ measurements (Grechnev et al. 2024). The proton flux was 255 pfu at energies > 10 MeV (Kocharov et al. 2018).

STEREO-A observed shock arrival on 18 May 2012, at 12:43 UT, with speed 793 km s^{-1}. The travel time to the spacecraft would be 35 hours, with mean speed of 1200 km s^{-1}. *Wind* observed shock arrival on 20 May 2012, at 01:20 UT, with speed 439 km s^{-1}. The travel time to the spacecraft would be 72 hours, with mean speed of 575 km s^{-1}. The time separation between the arrival times at STEREO-A and *Wind* was 37 hours.

4. Radio Emission and Source Heights

An essential part in comparing CME heights to radio source heights is the conversion from emission frequency to height. As plasma frequency depends only on the electron density in the surrounding medium, radio source heights can be calculated using atmospheric density models if the emission is plasma radiation. The different models are explained and compared in Pohjolainen et al. (2007); see their Table 1. In Al-Hamadani, Pohjolainen, and Valtonen (2017), height errors based on the model selection were estimated as 2.0 $R_{\odot}$ near 1 MHz, 1.0 $R_{\odot}$ near 500 kHz, and 0.3 $R_{\odot}$ near 150 kHz. This is based on the fact that as the frequency decreases, the height difference between the models decreases. At 10 MHz frequency, where the IP radio observations begin, the height difference between the most-extreme density models, Saito and 10-fold Saito, is 1.6 $R_{\odot}$ (Pohjolainen et al. 2007). The hybrid atmospheric density model by Vršnak, Magdalenić, and Zlobec (2004) is adopted in the current study, as the model starts from the high densities close to the Sun and also gives the low (measured) densities near Earth.

For wide-band emission, the next decision is which part of the emission lane should be used for height calculations. If we assume that the emission lane is widened by plasma processes, then we can use the emission lane center. If, however, the wide lane is produced by a shock front that extends to a large height range, for example, a bow shock along a curved CME front, then the emission lane borders can be used. For a fundamental-harmonic (F-H) lane pair, the F-lane should always be used in calculations.

CME propagation in the wake of earlier CMEs can change the atmospheric densities and hence affect the observed plasma frequencies during shock propagation. The 2003 halo CME was preceded by a narrow-width CME, which originated from the same active region, but it was not listed as a CME in the LASCO catalog as it had no clear moving front. The flow of the CME material is visible as a brightening in the coronagraph difference image at 22:30 UT, shown in Figure 4. The 2012 halo CME was preceded by other CMEs close in time, but interaction with them does not seem likely. One of them propagated up to 20 $R_{\odot}$, but the CME was directed northward and had narrow angular width of about 80 degrees. The other two CMEs were classified as poor events, which disappeared from the images near 10 $R_{\odot}$ height. They were directed southward and westward and had widths of 51 and 16 degrees, respectively. Plasma densities could have been affected by these structures, but not in a large scale.

The radio source heights calculated from the diffuse wide-band emission lane center and from the F-lane of the later, F-H part of the type II burst in the 2003 and 2012 events are shown in Figure 6. These height-time plots include the CME leading front heights observed by SOHO/LASCO and listed in the LASCO CME Catalog. For the 2003 event, the radio source heights are from *Wind*/WAVES observations (same viewing angle as for SOHO). For the 2012 event, the radio source heights are from STEREO-A/SWAVES observations, as Wind/WAVES did not observe the diffuse wide-band type II burst at all.

4.1. Diffuse Emissions in the 2003 and 2012 Radio Events

On 17 June 2003, the radio event started with a metric type II burst at 22:50 UT near 50 MHz; see the HiRAS spectrum in Figure 7 and NOAA spectral listings from Gulgoora and HiRAS. A metric type IV continuum appeared at the same time and continued until 23:50 UT. Both metric emissions could be recorded down to 20 MHz, but they did not continue to the *Wind*/WAVES frequencies.

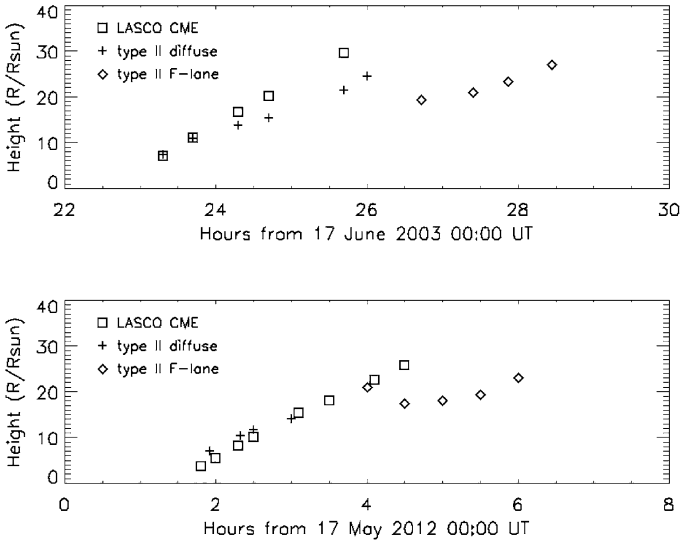

Figure 6 Height-times for the LASCO CME front (*squares*), diffuse wide-band emission lane center (*crosses*), and F-lane of the second part of the type II burst (*diamonds*), for the 17 – 18 June 2003 event (*top*) and 17 May 2012 event (*bottom*). Both plots show an eight-hour interval. The symbol size is 2 $R_\odot$, which represents the maximum error in radio source heights due to the use of atmospheric density models; see text for details.

The diffuse wide-band type II emission lane appeared in the dynamic spectrum at 23:00 UT, at 6 MHz center frequency. The heliocentric source height was ≈ 4.1 $R_\odot$, calculated from 6 MHz using the hybrid atmospheric density model. When the CME was first observed at 23:18 UT, the CME leading front was at height 7.06 $R_\odot$, and the diffuse wide-band type II burst at height 7.3 $R_\odot$. The duration of the diffuse emission was approximately three hours, and the emission lane could no longer be identified after 02:00 UT.

The separation between the CME heights and the diffuse emission source heights grew after 23:40 UT, and the diffuse radio source was located ≈ 7 $R_\odot$ lower than the CME leading front at 01:42 UT (last observation of the CME front, at 29.6 $R_\odot$). The growing height separation led Bastian (2007) to suggest that the diffuse emission could be due to incoherent synchrotron radiation, as there were difficulties in fitting the density variation of the diffuse component with time when assuming that it was plasma radiation associated with a CME-driven shock. The alternatives for the growing height separation would be an unusual density profile along the propagation path or a slow change in the location of the shock.

We calculated also radio burst heights by using the leading and trailing edges of the diffuse emission lane. Figure 7 shows a difference image of the CME at 00:18 UT with the calculated height range for the diffuse type II emission (region in between the green lines). The leading edge, at 400 kHz, has a height of 18 $R_\odot$, and the trailing edge, at 1 MHz, is at 10 $R_\odot$ height. Despite the height differences, and also when we take into account the differences between atmospheric density models, the diffuse type II burst heights follow the CME front heights quite well until 00:30 UT.

In the 17 May 2012 event metric type II emission was first observed at 01:32 UT near 50 MHz, followed by a metric type IV continuum; see HiRAS spectrum in Figure 8. Culgoora observations show the metric emissions as well, and they can be viewed, for example,

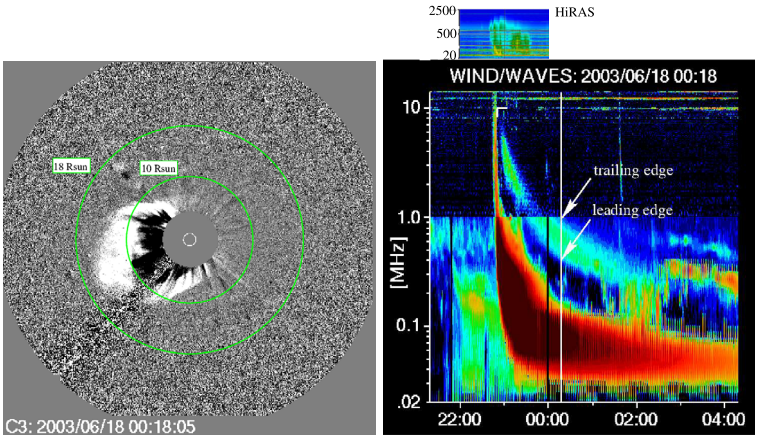

Figure 7 SOHO/LASCO-C3 difference image on 18 June 2003 at 00:18 UT. *Green circles* at heights 18 $R_\odot$ and 10 $R_\odot$ indicate the heights of the wide-band type II emission lane borders (leading and trailing edges of emission, respectively) at that time. The CME front covers these heights quite well. HiRAS dynamic spectrum (on *top*) shows a metric type II burst and a type IV continuum. These emissions did not continue to the *Wind*/WAVES frequencies.

in Grechnev et al. (2024). Both bursts look to continue to DH wavelengths, but the type IV burst was well observed only by STEREO-A.

The start time of the diffuse wide-band type II burst is uncertain due to the emission being mixed with strong type III bursts. The diffuse emission lane was observed only by STEREO-A. The lane becomes visible at 01:55 UT at 2 MHz, and the lane center corresponds to a height of 7.1 $R_\odot$. When the wide-band emission disappears from the spectrum at 03:00 UT, the lane center is at 600 kHz, and the estimated source height is 14.0 $R_\odot$. The duration of the diffuse emission is approximately one hour, i.e., much shorter than in the 2003 event. Some emission fragments, at various frequencies, are observed during 03:00 – 04:00 UT. We note that from the SOHO/LASCO viewing angle the diffuse emission lane was not observed at all (the white dashed line in the *Wind* dynamic spectrum in Figure 10 shows where the lane should have been).

The leading and trailing edge heights of the diffuse band emission are shown in Figure 8, indicated with green lines in the coronagraph images. The leading edge is at height 14.0 $R_\odot$ at 02:40 UT, which is higher than the CME front observed by SOHO/LASCO. The trailing edge of the diffuse emission, at 11.0 $R_\odot$, is very near the LASCO-C3 CME front height (11.5 $R_\odot$). As is shown in Figure 6, the diffuse type II center-lane heights follow the LASCO CME leading front heights quite well. The height difference can be explained by taking into account projection effects for the CME and a possible 2 $R_\odot$ error in determining radio source heights.

In the STEREO-A view the CME front is at much lower height (8.6 $R_\odot$) than the diffuse type II emission at 02:40 UT (11.0 – 14 $R_\odot$). This could simply be due to the CME nose being directed toward STEREO-A, as then STEREO-A would only see the CME flanks projected on the sky. In Section 5 the possibility of two separate CMEs and shocks is discussed further.

In the STEREO-A/COR2 white-light images a sharp edge of diffuse emission is visible in the north-eastern part of the CME, indicated with arrows in Figure 8. This type of feature can be interpreted as a density enhancement from a fast-mode MHD shock (Vourlidas et al.

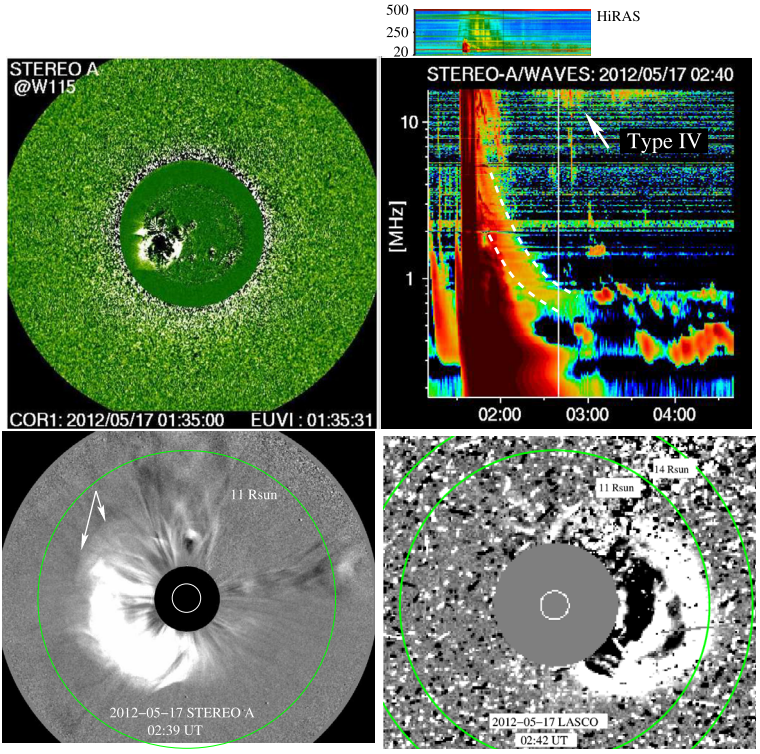

Figure 8 In the 2012 event, STEREO-A/EUVI observed an EUV wave at 01:35 UT (*top left*). STEREO-A dynamic spectrum shows a diffuse type II burst (leading and trailing edges indicated with *dashed lines*) and a type IV burst. HiRAS dynamic spectrum on top shows a metric type II burst and a type IV continuum. The CME was observed by STEREO-A/COR2 at 02:39 UT on 17 May 2012 (*bottom left*) and by SOHO/LASCO-C3 at 02:42 UT (*bottom right*). The height range of the diffuse wide-band type II burst was $11-14\ R_{\odot}$ near those times, and these heights are indicated with *green circles* on the coronagraph images. In the STEREO-A difference image at 02:39 UT, *arrows* point to the white-light shock region formed in the north-eastern part of the CME leading front.

2003). The white-light shock heights are similar to the STEREO-A CME heights. The speed of the white-light shock front, approximately 1100 km s^{-1}, is slightly higher than the speed of the visible STEREO-A CME front (that may not be the real front), 1000 km s^{-1}.

This sharp-edged shock region is visible also in the STEREO-B images, although at much lower heights, as from this viewing angle the shock is moving away from the observer. In the SOHO/LASCO field-of-view the white-light shock structure is located in the north-western side of the CME; see, for example, Figure 4 in Gopalswamy et al. (2013).

STEREO-A dynamic spectrum shows a type IV burst from 02:25 UT until 03:50 UT, at frequencies higher than 12 MHz, which looks to be a continuation of the metric type IV emission. A type IV burst is typically an indication of flare-accelerated electrons trapped in post-flare loops or CME structures, and the radiation is due to either synchrotron or plasma emission, or both; see, for example, Talebpour Sheshvan and Pohjolainen (2018) and references therein. The type IV burst disappears from the spectrum near the time when the F-lane emission starts. Type IV bursts are known to show directivity effects, i.e., the emission is visible only if the source region is located within 60° from the solar disc center (Mohan et al.

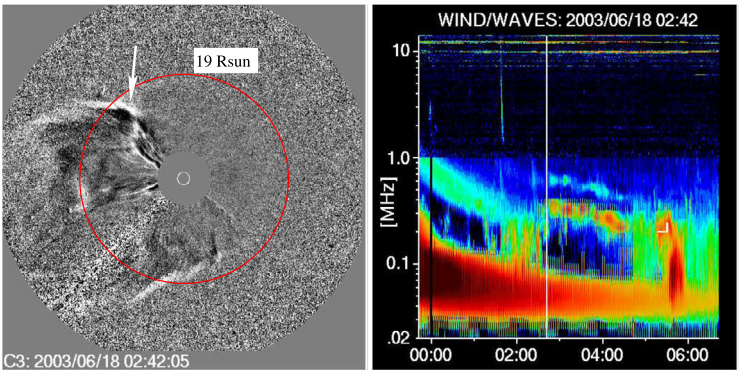

Figure 9 CME shape near the start time of the F-H emission lane pair on 18 June 2003 at 02:42 UT. The F-lane radio emission starts at 360 kHz, which corresponds to a height of about 19 $R_\odot$. This height is indicated with a *red circle* in the LASCO-C3 difference image. The most-affected streamer region is marked with an *arrow*.

2024). This is the case also here, as the IP type IV burst is observed only in the STEREO-A view, at source longitude E42.

4.2. F-H Plasma Emissions in the 2003 and 2012 Radio Events

In the 2003 radio event, the F-H emission lane pair became visible near 02:40 UT on 18 June, and after 04:30 UT, the lane pair could no longer be identified among other intense emissions (Figure 9). The F-lane of the burst drifted from 360 kHz to 230 kHz, which corresponds to heliocentric heights from 19.3 $R_\odot$ to 27.0 $R_\odot$. The CME leading front could no longer be observed when the F-H lane pair appeared in the dynamic spectrum, but from the extrapolated CME heights the difference to the F-lane height at 02:43 UT was ≈ 20 $R_\odot$. The CME shape near the start time of the F-H lane emission is shown in Figure 9, and the red line indicates the radio F-lane source height at 19.0 $R_\odot$. At that height, we also see a bending of a streamer on the north-eastern flank of the CME.

In the 2012 radio event, the F-H emission lane pair is clearly visible during 05:00 – 06:00 UT on 17 May. However, the emission between 04:00 UT and 05:00 UT, which looks to belong to the F-lane, does not show clear H-lane emission (Figure 10, the start of F-H emission is indicated in both *Wind* and STEREO-A dynamic spectra). The observed emissions drift from 320 kHz at 04:00 UT to 280 kHz at 06:00 UT, corresponding to heliocentric heights from 21.0 $R_\odot$ to 23.1 $R_\odot$. However, the curvature of emission toward the higher frequencies could be a visual effect if the emission at 04:00 – 05:00 is not part of the F-H type II burst.

The F-lane source heights after 05:00 UT match quite well with the heights of the CME front observed by STEREO-A, and the white-light shock region could propagate along the same height-time path; see Figure 11. The CME leading front heights could be estimated from the STEREO-A/HI1-A images at heights larger than 15 $R_\odot$, but the white-light shock front was visible only in the STEREO-A/COR2 images.

5. Summary and Conclusions

This study reports on two similar-looking, two-part interplanetary (IP) radio type II burst events from 2003 and 2012. In these events, a diffuse wide-band type II burst was followed

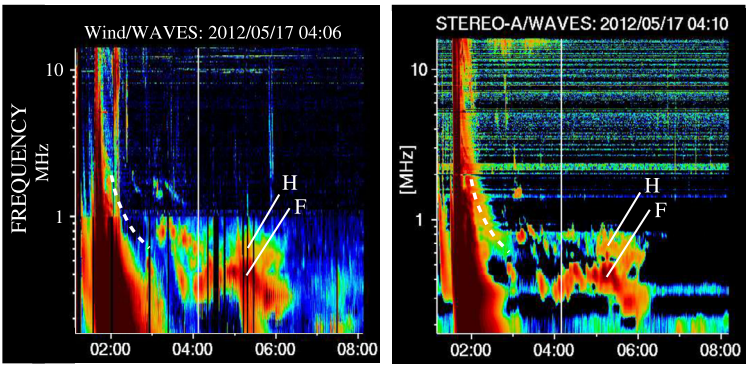

Figure 10 Comparison between the *Wind*/WAVES and STEREO-A/SWAVES dynamic spectra. *Dashed white line* indicates the frequencies of the emission lane center of the diffuse wide-band type II burst. The diffuse type II burst and the type IV burst are not visible in the *Wind*/WAVES spectrum; they show up only in the STEREO-A observations. The F-H type II burst lanes look almost identical, but the existence of the lane pair is uncertain before 05:00 UT.

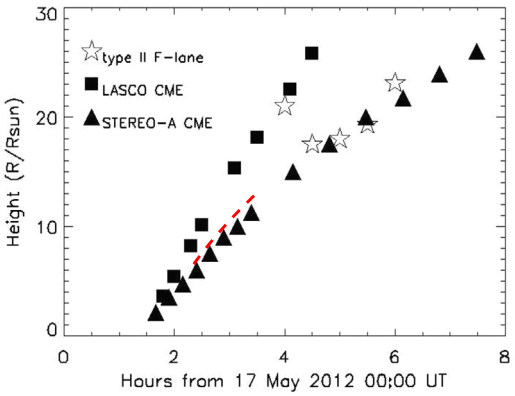

Figure 11 CME heights from SOHO/LASCO (C2 and C3) and from STEREO-A/SECCHI (COR1, COR2, and HI) for the 17 May 2012 event. The STEREO-A CME front heights are similar to the heights of the white-light shock region located in the north-eastern part of the CME leading front, the shock region heights are indicated with a *red dashed line* (COR2 observations only). Estimated heights for the F-lane of the type II burst are shown with *star symbols*. The H-lane of the burst appeared only after 05:00 UT.

by a type II burst that shows fundamental and harmonic (F-H) emission lanes, both of which are slightly curved in their frequency-time evolution.

The change from a diffuse wide-band lane to narrow F-H bands is not typical for IP type II bursts. Of the 25 wide-band type II events from 2001 – 2011 presented in Pohjolainen, Allawi, and Valtonen (2013), only a few suggest such evolution. The 2003 event was listed there as event number 9, and most of the bursts occurred before STEREO observations. As the newer 2012 event was observed from three different viewing angles, we could here compare the observations from each spacecraft.

The associated halo-type CMEs in the 2003 and 2012 events showed similar shapes and structures. In both events, the elongated CME fronts had heights that match with the wide-band diffuse type II emission if we consider the whole emission lane and not just the lane

center. However, in the 2003 event, there was a growing height separation between the CME leading front and the diffuse type II emission source after the first hour of propagation. In the 2012 event, similar evolution may be present, but as in this event the diffuse emission was present only for about one hour, compared to the three hours in the 2003 event, it is uncertain.

If the diffuse type II emission is plasma radiation and not synchrotron emission as it has sometimes been suggested, then only the atmospheric densities and source heights determine the emitting frequencies. If the heights of the diffuse emission fell behind the heights of the CME leading front at later times, this could be due to untypical changes in the atmospheric densities or the shock location changed in time. The widening of the emission band could correspond to a larger emission region, or it could be explained by a larger density gradient at the radio source region. Similarly, if the source region narrowed and changed position, then it would affect the appearance of the diffuse emission. For example, Iwai et al. (2020) found a positive correlation between the type II bandwidth and SEP peak flux, supporting the idea that if particle acceleration occurs on a larger spatial scale, the more SEPs will be generated.

In these two events, the diffuse type II burst weakens and disappears from the spectrum before or near the time when the F-H type II burst is formed. In the statistical study, Pohjolainen, Allawi, and Valtonen (2013) found that in most cases the diffuse emission continues much longer, and it can be followed to much lower frequencies. Hence it could be possible that the formation of the F-H type II burst is somehow connected to the early ending of the diffuse radio emission. For example, the wide leading front of the CME could break up, causing the shock region to move down on the CME side, to a more narrow region. Or, if the diffuse type II burst was synchrotron emission, then its cessation made it possible for the F-H type II burst to appear in the spectrum.

In both events, the F-H type II burst heights are much lower than the highest observed CME front heights. A simple explanation would be that a separate flank shock is formed at lower heights, due to the lateral CME expansion and collision with a streamer. In the 2003 event a flank shock looks probable, as we see a bending streamer near the heights of the F-H type II burst. This could also explain the curvature of the F-H emission lanes: at the CME flanks the atmospheric densities are first lower, but when the shock meets increased streamer densities, the emission frequency increases. When the shock region moves forward, the shock propagates back into decreasing densities.

In the 2012 event, there are emission structures present after the ending of the diffuse radio burst and before the appearance of the F-H burst, which do not look to belong to either of the bursts. In this event the white-light imaging observations do not show any clear indication of interaction with streamers.

In the earlier analysis of the 2012 event, Shen et al. (2013) suggested that the event consisted of two separate CMEs. In another study, Grechnev et al. (2024) identified two wave-like disturbances, which later merged into a halo-shock. Therefore they fitted the observed radio emissions with three separate type II bursts (Figure 19 in their paper). Basically, their 1F-H is a continuation of the metric type II burst, their 3F corresponds to our diffuse type II lane, and their 2F-H is located in between them. Grechnev et al. (2024) also suggested that at distances exceeding ten solar radii the piston shock was transformed into a bow shock.

Based on our current analysis and the earlier studies on the 2003 and 2012 events, the hypothesis for the two-part interplanetary type II bursts are:

- A bow-shock is formed along the leading front of a CME, creating a wide-band type II burst. The bow shock dies out when the front separates into multiple loops. At heights $\approx 20\ R_{\odot}$, a CME flank shock is formed, with interaction with a nearby streamer.

The F-H type II emission from the flank shock reflects the varying densities within the streamer region.

- Alternatively, together with the bow-shock that creates the wide-band type II burst, a second global shock is formed at the same time. Due to plasma and possible viewing angle effects, the F-H type II shock becomes visible only later, at heights ≈ 20 $R_\odot$.
- Third possible scenario is that the eruption creates two CME fronts that propagate to slightly different directions with different speeds. The fast and wide CME front creates the diffuse wide-band type II burst, and the slower CME creates the F-H type II burst later on.

In the 2003 event, a bow shock with a later flank shock and interaction with a streamer looks possible. We found no evidence of more than one CME or other white-light shocks, but as the existing observations were limited to one field-of view, with gaps in the coronagraph imaging, this result can still be questioned. We cannot either rule out the possibility that the diffuse emission was caused by synchrotron radiation.

In the 2012 event, the wide-band diffuse type II emission was observed only in the STEREO-A view. The CME height was, however, lower in the STEREO-A view than in the SOHO/LASCO view. This height difference could simply be due to the CME front being directed more toward STEREO-A, and LASCO would observe the front better from a side angle. The existence of IP type IV radio emission, but only in the STEREO-A view, also indicates a rising CME structure that is moving toward STEREO-A. The diffuse radio type II burst emission agrees with a propagating CME bow shock, in heights and speed, and an in situ shock was observed to arrive at STEREO-A in a time-frame comparable to the CME speed.

The STEREO-A coronagraph images also show a white-light shock region located on the north-eastern side of the CME. This suggests a simultaneous existence of a CME bow shock at LASCO heights and a second, global shock at STEREO-A heights. Comparison between the STEREO-A shock heights and the later-appearing F-H type II burst heights suggest that the F-H type II burst could have been created by this shock. The propagation speed of the shock structure was approximately 1100 km s^{-1}. With deceleration, it could match with the shock arrival near Earth 72 hours later. However, as the tracking of the white-light shock region can be done only up to the COR2 coronagraph height limit of 15 $R_\odot$, we do not know what happens to the shock after that.

So the following question remains open: are there two CMEs that create two propagating shocks in the 2012 event that move at different speeds to slightly different directions, or is there just one CME that creates two separate shocks? A fast and wide CME, directed toward the observing instrument, would create a CME bow shock that shows up as a diffuse wide-band type II burst. For the later-appearing F-H type II burst, we cannot rule out the possibility of a second CME, although the one-CME and two-shock scenario does have observational support.

6. Discussion

Repeated events and similarities in emission structures have always been of interest, especially for prediction purposes. Homologous CMEs that eject similar structures repeatedly from the same source region have been reported by Bian et al. (2022). Then homologous solar flares present features that are most likely due to similarities in the magnetic field configurations and particle acceleration processes; see, for example, Romano et al. (2018) and references therein. Particle beams and propagating shock waves create plasma emission via

nonlinear wave-wave interactions, but the emission contains also various radio wave propagation effects in the inhomogeneous and turbulent corona (Kontar et al. 2019), which need to be taken into account.

Several studies that have used radio triangulation and 3D reconstruction techniques have concluded that most of the type II burst sources are located at the flanks of the CMEs (Magdalenić et al. 2014; Hu et al. 2016; Krupar et al. 2016). Interaction with a streamer has often been suggested to be causing the type II burst. In addition, Jebaraj et al. (2020) found that one CME could be the driver of two separate type II bursts, but the bursts appeared at different parts of the CME and at different flanks.

Trapped particles, indicated by the existence of radio type IV bursts, could also affect the detected SEP populations. Recently, Jebaraj et al. (2024) presented the first-ever direct measurements of synchrotron-emitting heliospheric traveling shocks, intercepted by the Parker Solar Probe during its close encounters. They found that strong quasi-parallel shocks are better emitters of radiation than quasi-perpendicular shocks due to the efficient acceleration of ultra-relativistic electrons. Hence it is of interest whether these shocks show up as the diffuse wide-band type II bursts or if the efficient acceleration is associated with the later, F-H part of type II burst events.

In the analysed 2012 event, the F-H type II burst was observed by STEREO-A and *Wind*, in contrast to the diffuse type II and type IV bursts, which were observed only by STEREO-A. Moreover, the type IV burst ended near the time when the F-H burst appeared. This may suggest something similar to the cases presented by Pohjolainen and Talebpour Sheshvan (2020), where a lower-located type IV burst source is most visible when there is no shock front in between the type IV source and the observer. A shock region producing a type II burst could then act as an absorber, not letting the type IV emission come through.

The observed directionality of type IV bursts, i.e., they are observed only when the source is viewed top-on along the direction of propagation (Talebpour Sheshvan and Pohjolainen 2018), bears some similarities with the diffuse type II emission. Type IV bursts are thought to be a combination of synchrotron and plasma emission, a magnetic cloud containing trapped particles and moving outward in the solar atmosphere, but the reason for not observing them from all viewing angles is still unclear. The same now applies to at least some diffuse IP type II bursts. The simplest explanation in both plasma and synchrotron cases would be that the emission is observed when nothing blocks or absorbs the radio waves along the line-of-sight.

As we do not have radio imaging observations at DH wavelengths, the actual radio source locations cannot be observed directly. The radio triangulation technique and direction-finding observations have been used as an indirect imaging tool in some cases (see Jebaraj et al. (2021) and references therein), but a more systematic and simple tool would be needed to explain the still unknown features and physical processes that occur associated with IP type II solar radio bursts.

Acknowledgements Special thanks go to the people who have built and maintained the various solar data archives, who contributed in creating and updating the solar event catalogues and thus enabled easy access to various data products. The CDAW CME catalogue is generated and maintained at the CDAW Data Center by NASA and the Catholic University of America in cooperation with the Naval Research Laboratory. SOHO is a project of international cooperation between ESA and NASA. STEREO is part of the NASA Solar Terrestrial Probes (STP) Program. The comments and suggestions made by the anonymous reviewer helped to improve the presentation and content of this work.

Author contributions S.P. did the data analysis, prepared the figures, and wrote the manuscript.

Funding Information Open Access funding provided by University of Turku (including Turku University Central Hospital).

Data Availability No datasets were generated or analysed during the current study.

Declarations

Competing interests The authors declare no competing interests.

References

Al-Hamadani, F., Pohjolainen, S., Valtonen, E.: 2017, Origin of radio enhancements in type II bursts in the outer corona. *Solar Phys.* **292**, 127. DOI.

Bastian, T.S.: 2007, Synchrotron radio emission from a fast halo coronal mass ejection. *Astrophys. J.* **665**, 805. DOI.

Bian, X., Jiang, C., Feng, X., Zuo, P., Wang, Y.: 2022, Homologous coronal mass ejections caused by recurring formation and disruption of current sheet within a sheared magnetic arcade. *Astrophys. J. Lett.* **925**, L7. DOI.

Bougeret, J.-L., Kaiser, M.L., Kellogg, P.J., Manning, R., Goetz, K., Monson, S.J., Monge, N., Friel, L., Meetre, C.A., Perche, C., Sitruk, L., Hoang, S.: 1995, WAVES: the radio and plasma wave investigation on the wind spacecraft. *Space Sci. Rev.* **71**, 231. DOI.

Bougeret, J.-L., Goetz, K., Kaiser, M.L., Bale, S.D., Kellogg, P.J., Maksimovic, M., et al.: 2008, S/WAVES: the radio and plasma wave investigation on the STEREO mission. *Space Sci. Rev.* **136**, 487. DOI.

Cane, H.V., Erickson, W.C.: 2005, Solar type II radio bursts and IP type II events. *Astrophys. J.* **623**, 1180. DOI.

Chernov, G., Fomichev, V.: 2021, On the issue of the origin of type II solar radio bursts. *Astrophys. J.* **922**, 82. DOI.

Domingo, V., Fleck, B., Poland, A.I.: 1995, SOHO: the solar and heliospheric observatory. *Space Sci. Rev.* **72**, 81. DOI.

Dulk, G.A.: 1985, Radio emission from the sun and stars. *Annu. Rev. Astron. Astrophys.* **23**, 169. DOI.

Feng, S.W., Chen, Y., Kong, X.L., Li, G., Song, H.Q., Feng, X.S., Liu, Y.: 2012, Radio signatures of coronal-mass-ejection-streamer interaction and source diagnostics of type II radio burst. *Astrophys. J.* **753**, 21. DOI.

Gopalswamy, N., Mäkelä, P., Yashiro, S.: 2019, A catalog of type II radio bursts observed by wind/WAVES and their statistical properties. *Sun Geosph.* **14**, 111. DOI.

Gopalswamy, N., Xie, H., Akiyama, S., Yashiro, S., Usoskin, I.G., Davila, J.M.: 2013, The first ground level enhancement event of solar cycle 24: direct observation of shock formation and particle release heights. *Astrophys. J. Lett.* **765**, L30. DOI.

Grechnev, V.V., Kiselev, V.I., Uralov, A.M., Meshalkina, N.S., Firoz, K.A., Lysenko, A.L.: 2024, Mysteries of the 17 May 2012 solar event responsible for GLE71. I. CME development and the role of disturbances excited by eruptions. *Solar Phys.* **299**, 129. DOI.

Hillaris, A., Bouratzis, C., Nindos, A.: 2016, Interplanetary type IV bursts. *Solar Phys.* **291** 2049. DOI.

Hu, H., Liu, Y.D., Wang, R., Möstl, C., Yang, Z.: 2016, Sun-to-Earth characteristics of the 2012 July 12 coronal mass ejection and associated geo-effectiveness. *Astrophys. J.* **829**, 97. DOI.

Iwai, K., Yashiro, S., Nitta, N.V., Kubo, Y.: 2020, Spectral structures of type II solar radio bursts and solar energetic particles. *Astrophys. J.* **888**, 50. DOI.

Jebaraj, I.C., Magdalenić, J., Podladchikova, T., Scolini, C., Pomoell, J., Veronig, A.M., Dissauer, K., Krupar, V., Kilpua, E.K.J., Poedts, S.: 2020, Using radio triangulation to understand the origin of two subsequent type II radio bursts. *Astron. Astrophys.* **639**, A56. DOI.

Jebaraj, I.C., Kouloumvakos, A., Magdalenic, J., Rouillard, A.P., Mann, G., Krupar, V., Poedts, S.: 2021, Generation of interplanetary type II radio emission. *Astron. Astrophys.* **654**, A64. DOI.

Jebaraj, I.C., Agapitov, O.V., Gedalin, M., Vuorinen, L., Miceli, M., Vainio, R., Cohen, C.M.S., Voshchepynets, A., Kouloumvakos, A., Dresing, N., Marmyleva, A., Krasnoselskikh, V., Balikhin, M., Mitchell, J.G., Labrador, A.W., Wijsen, N., Palmerio, E., Colomban, L., Pomoell, J., Kilpua, E.K.J.: 2024, Direct measurements of synchrotron-emitting electrons at near-sun shocks. *Astrophys. J. Lett.* **976**, L7. DOI.

Jian, L.K., Russell, C.T., Luhmann, J.G., Galvin, A.B.: 2018, STEREO observations of interplanetary coronal mass ejections in 2007 – 2016. *Astrophys. J.* **855**, 114. DOI.

Jin, M., Cheung, M.C.M., DeRosa, M.L., Nitta, N.V., Schrijver, C.J.: 2022, Coronal mass ejections and dimmings: a comparative study using MHD simulations and SDO observations. *Astrophys. J.* **928**, 154. DOI.

Kaiser, M.L., Kucera, T.A., Davila, J.M., St. Cyr, O.C., Guhathakurta, M., Christian, E.: 2008, The STEREO mission: an introduction. *Space Sci. Rev.* **136**, 5. DOI.

Kocharov, L., Pohjolainen, S., Reiner, M.J., Mishev, A., Wang, H., Usoskin, I., Vainio, R.: 2018, Spatial organization of seven extreme solar energetic particle events. *Astrophys. J.* **862**, L20. DOI.

Kontar, E.P., Chen, X., Chrysaphi, N., Jeffrey, N.L.S., Emslie, A.G., Krupar, V., Maksimovic, M., Gordovskyy, M., Browning, P.K.: 2019, Anisotropic radio-wave scattering and the interpretation of solar radio emission observations. *Astrophys. J.* **884**, 122. DOI.

Krupar, V., Eastwood, J.P., Kruparova, O., Santolik, O., Soucek, J., Magdalenić, J., Vourlidas, A., Maksimovic, M., Bonnin, X., Bothmer, V., Mrotzek, N., Pluta, A., Barnes, D., Davies, J.A., Martínez Oliveros, J.C., Bale, S.D.: 2016, An analysis of interplanetary solar radio emissions associated with a coronal mass ejection. *Astrophys. J. Lett.* **823**, L5. DOI.

Kumari, A., Morosan, D.E., Kilpua, E.K.J., Daei, F.: 2023, Type II radio bursts and their association with coronal mass ejections in solar cycles 23 and 24. *Astron. Astrophys.* **675**, A102. DOI.

Magdalenić, J., Marqué, C., Krupar, V., Mierla, M., Zhukov, A.N., Rodriguez, L., Maksimović, M., Cecconi, B.: 2014, Tracking the CME-driven shock wave on 2012 March 5 and radio triangulation of associated radio emission. *Astrophys. J.* **791**, 115. DOI.

Mann, G., Warmuth, A., Önel, H.: 2023, Kinematical evolution of large-scale EUV waves in the solar corona. *Astron. Astrophys.* **675**, A129. DOI.

Mann, G., Vocks, C., Warmuth, A., Magdalenic, J., Bisi, M., et al.: 2022, Excitation of Langmuir waves at shocks and solar type II radio bursts. *Astron. Astrophys.* **660**, A71. DOI.

Melrose, D.B.: 1987, Plasma emission: a review. *Solar Phys.* **111**, 89. DOI.

Mohan, A., Gopalswamy, N., Kumari, A., Akiyama, S., Sindhuja, G.: 2024, Interplanetary type IV solar radio bursts: a comprehensive catalog and statistical results. *Astrophys. J.* **971**, 86. DOI.

Müller, D., Nicula, B., Felix, S., Verstringe, F., Bourgoignie, B., Csillaghy, A., Berghmans, D., Jiggens, P., García-Ortiz, J.P., Ireland, J., Zahniy, S., Fleck, B.: 2017, JHelioviewer. Time-dependent 3D visualisation of solar and heliospheric data. *Astron. Astrophys.* **606**, A10. DOI.

Pohjolainen, S., Allawi, H., Valtonen, E.: 2013, Origin of wide-band IP type II bursts. *Astron. Astrophys.* **558**, A7. DOI.

Pohjolainen, S., Pomoell, J., Vainio, R.: 2008, CME liftoff with high-frequency fragmented type II burst emission. *Astron. Astrophys.* **490**, 357. DOI.

Pohjolainen, S., Talebpour Sheshvan, N.: 2020, Cut-off features in interplanetary solar radio type IV emission. *Adv. Space Res.* **65**, 1663. DOI.

Pohjolainen, S., van Driel-Gesztelyi, L., Culhane, J.L., Manoharan, P.K., Elliott, H.A.: 2007, CME propagation characteristics from radio observations. *Solar Phys.* **244**, 167. DOI.

Romano, P., Elmhamdi, A., Falco, M., Costa, P., Kordi, A.S., Al-Trabulsy, H.A., Al-Shammari, R.M.: 2018, Homologous white light solar flares driven by photospheric shear motions. *Astrophys. J. Lett.* **852**, L10. DOI.

Shen, C., Li, G., Kong, X., Hu, J., Sun, X.D., Ding, L., Chen, Y., Wang, Y., Xia, L.: 2013, Compound twin coronal mass ejections in the 2012 May 17 GLE event. *Astrophys. J.* **763**, 114. DOI.

Talebpour Sheshvan, N., Pohjolainen, S.: 2018, Visibility and origin of compact interplanetary radio type IV bursts. *Solar Phys.* **293**, 148. DOI.

Vourlidas, A., Wu, S.T., Wang, A.H., Subramanian, P., Howard, R.A.: 2003, Direct detection of a coronal mass ejection-associated shock in large angle and spectrometric coronagraph experiment white-light images. *Astrophys. J.* **598**, 1392. DOI.

Vršnak, B., Magdalenić, J., Zlobec, P.: 2004, Band-splitting of coronal and interplanetary type II bursts. III. Physical conditions in the upper corona and interplanetary space. *Astron. Astrophys.* **413**, 753. DOI.